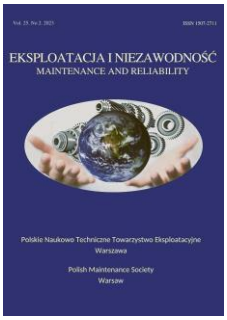

Eksploatacja i Niezawodnosc – Maintenance and Reliability

Volume 28 (2026), Issue 3

journal homepage: http://www.ein.org.pl

Article citation info:
La QT, Vališ D, Vintr Z, Gajewski J, Žák L, Kohl Z, Cu XP, An approach to analyse of LED degradation heterogeneity in step-stress accelerated testing, Eksploatacja i Niezawodnosc – Maintenance and Reliability 2026: 28(3) http://doi.org/10.17531/ein/217551

An approach to analyse of LED degradation heterogeneity in step-stress accelerated testing

Indexed by: Web of Science Group

Quoc Tiep La[a,*], David Vališ[a], Zdeněk Vintr[a], Jakub Gajewski[b], Libor Žák[c], Zdeněk Kohl[a], Xuan Phong Cu[d]

[a] Faculty of Military Technology, University of Defence, Czech Republic
[b] Faculty of Mechanical Engineering, Lublin University of Technology, Poland
[c] Brno University of Technology, Czech Republic
[d] Le Quy Don Technical University, Viet Nam

Highlights

- Optimised step-stress accelerated testing captures LED degradation behaviour.
- Empirical Mode Decomposition extracts degradation trends and separates noise.
- Kernel density estimation models cross-device degradation feature distributions.
- Divergence measures quantify cross-device heterogeneity.

Abstract

Light-emitting diodes (LEDs) have become indispensable in modern applications owing to their high energy efficiency, long lifespan, and robustness compared to conventional light sources. Given these attributes, the reliability of LEDs has become a crucial factor, directly influencing the ability of systems and devices to perform their intended functions over time. However, variations in materials, structures, and manufacturing processes introduce heterogeneity in their degradation behaviour, even under identical operating conditions. In applications demanding brightness stability, colour rendering, and reliability prediction, degradation homogeneity is crucial, making the analysis of LED heterogeneity essential. This article investigates such heterogeneity using feature extraction methods, kernel density estimation, and divergence measures based on degradation data obtained from optimized step-stress accelerated tests. The proposed approach is used to quantify and evaluate LED degradation variability and has clear implications for reliability assessment and predictive modelling.

Keywords
light emitting diode, reliability, degradation process, step-stress accelerated test, degradation heterogeneity

1. Introduction

Light sources play a fundamental role across diverse domains, including engineering, economics, medicine, and daily life applications. Their wide applicability has driven continuous research and development to meet the growing demand for efficiency, durability, and sustainability. Among modern lighting technologies, LEDs have emerged as the dominant solution, offering significant advantages over conventional light sources. These advantages include high luminous efficiency, compact design, ease of replacement, reduced energy consumption, and an extended operational lifetime of up to 50,000 hours under standard conditions [1]. Given these attributes, the reliability of LEDs has become a crucial factor, directly influencing the ability of systems and devices to perform their intended functions over time.

(*) Corresponding author.
E-mail addresses: QT. La (ORCID: 0000-0002-4809-737X) quoctiep.la@unob.cz, D. Vališ (ORCID: 0000-0002-3911-2689) david.valis@unob.cz, Z. Vintr (ORCID: 0000-0003-3128-0802) zdenek.vintr@unob.cz, J. Gajewski (ORCID: 0000-0001-8166-7162) j.gajewski@pollub.pl, L. Žák (ORCID: 0000-0001-6408-5646) zak.l@fme.vutbr.cz, Z. Kohl (ORCID: 0000-0003-2131-1927) zdenek.kohl@unob.cz, XP. Cu (ORCID: 0009-0007-1589-5862) phong.cx@lqdtu.edu.vn

Advances in sensor technologies and measurement systems have enabled monitoring of degradation for reliability assessment based on collected data [2], rather than waiting for failures. However, obtaining reliability data under normal conditions is time-consuming and costly, especially for long-lived, highly reliable products such as LEDs [3]. Accelerated testing (AT) addresses this challenge by applying harsher stresses or higher loads to shorten test duration, and provide insights into degradation mechanisms and facilitating lifetime prediction [4]. Existing standard [5] provided frameworks to conduct ATs for LED, while [6] provide a framework to enable lifetime assessment. In practice, Zhang et al. [7] applied constant electrical stresses to multiple LED groups, monitoring lumen depreciation with probabilistic lifetime models, whereas Herzog et al. [8] examined spectral degradation of high-power COB LEDs under prolonged constant thermal stress. Similarly, Alsharabi et al. [9] evaluated InGaN blue LEDs under simultaneous thermal, electrical, and humidity stresses. In another related investigation, Fan et al. [10] adopted stochastic degradation models to predict lifetime of UV LEDs based on data from constant stress and step stress degradation tests, and Lokesh [11] conducted ATs for cool white LEDs under three thermal stress level and constant drive current and proposed a colorimetric approach based on chromaticity shifts. In parallel, Xia et al. [12] explored gamma irradiation effects on UVC LEDs, while Yan et al. [13] conducted highly accelerated electrical stressing at low temperatures for GaN-based LEDs. More complex multi-stress tests, including thermal–electrical cycling, have been reported in [14-16]. Collectively, these studies demonstrate the diversity of AT designs and highlight the importance of selecting stress profiles, reflecting practical operating conditions.

Among the ATs, step-stress accelerated degradation testing (SSADT) significantly reduces the time and cost required to collect reliability data, especially for highly reliable products that take a long time to fail under normal conditions. By subjecting units to successively increasing stress levels, the method ensures that degradation at lower stress levels is captured prior to overstressing while subsequently accelerating the failure process at higher stress levels, allowing long-term reliability estimates to be made in a much shorter timeframe [17]. In LED reliability research, SSADT has become an important approach for collecting degradation data efficiently. Do et al. [18] conducted an SSADT to monitor optical intensity of medical LEDs, while Zhang et al. [19] employed constant-stress and step-stress electrical tests to obtain OLED brightness degradation and proposed a statistical method for lifetime estimation. Moreover, Jing et al. [20] collected emission-power degradation data for UV LEDs under thermal and stepped electrical stresses and analysed the resulting trajectories using TM-21 and an asymptotic Wiener-process framework for remaining useful life (RUL) estimation. In another aspect, Cai et al. [21] introduced a highly accelerated decay testing procedure to identify thermal-stress limits under humidity constraints and validated the degradation mechanism through SSADT. Additional SSADT-based studies can be found in [10,22].

Despite its flexibility, the informativeness of SSADT data strongly depends on the selected stress sequence, duration, and transition points. Suboptimal choices may limit the amount of usable degradation information, inflate parameter uncertainty, or violate the assumed acceleration mechanism. Therefore, a rigorously designed test plan is required. Nelson et al. [4] provides a foundational framework for constructing optimal test plans using statistical modelling, Fisher information, and sensitivity analysis, emphasizing that stress levels, durations, and sample allocation should be chosen to maximize information about acceleration-model parameters. Building on this principle, Wang et al. [23] proposed an optimization scheme for Wiener-process-based SSADTs by enforcing mechanism equivalence across stress levels. Their algorithm extracts valid degradation information and employs an M-optimality criterion to identify optimal transition times for LED thermal-stress SSADTs. In another approach, Sun et al. [24] developed an SSADT optimization method for the Birnbaum–Saunders model, aimed at minimizing prediction mean squared error under cost constraints via Monte Carlo simulation, leading to optimal decisions on sample size and measurement scheduling. Meanwhile, Liu et al. [25] further advanced SSADT optimization using a hybrid neural-network–genetic-algorithm strategy, allowing simultaneous optimization of stress levels, durations, and other design parameters while accounting for both accelerated-stress effects and measurement error. Sensitivity analyses in their work highlight key parameters

influencing design robustness. The above analysis shows that designing an optimized SSADT for LEDs is crucial. This ensures that the collected degradation data are both statistically informative and physically representative, enabling accurate reliability assessment and precise lifetime prediction under realistic operating conditions.

At this point, it is also important to consider heterogeneity, which plays a key role in reliability assessment. In the context of LED degradation, heterogeneity refers to significant variations in degradation rates, lifetime, and overall reliability among nominally identical units under identical operating conditions. Such variability arises from manufacturing imperfections, material inconsistencies, and minor deviations in operating modes [26]. Numerous studies have highlighted the impact of unit-to-unit heterogeneity on reliability. For example, Zheng et al. [27] employed an inverse Gaussian process with Gamma-distributed random effects to capture heterogeneity in torsion springs and integrated circuits, while Junxing et al. [28] extended Wiener-based stochastic models to account for variability across units. Wen et al. [29] focused on multiphase degradation processes separated by change points rather than unit heterogeneity. In LEDs, where precise brightness and color rendering are critical, capturing heterogeneity is essential. Veloso et al. [30] applied Bayesian dynamic linear degradation models to infrared LEDs, and Hoang et al. [14] introduced a Wiener-based model incorporating unit-to-unit covariates for high-power LEDs. Complementary studies [31,32] further explored heterogeneity under varying currents, optical conditions, and junction temperature measurements. These findings collectively indicate that heterogeneity, both across units and within multiphase degradation, is inherent to LED degradation and must be explicitly incorporated into reliability modelling, yet quantitative investigations remain limited.

Heterogeneity in degradation of LEDs is widely recognised, quantitative assessment of heterogeneity remains limited, which can compromise the accuracy and reliability of lifetime predictions. While optical metrics such as luminous flux and colour shift are commonly used in standards like TM-21 [33], electrical parameters, particularly forward voltage, provide a complementary perspective on degradation and allow a continuous, high-resolution indicator for quantifying degradation across units [14, 34]. SSADT, potentially combined with optimised test plans, enables efficient collection of degradation trajectories that support rigorous, quantitative evaluation of heterogeneity. This motivates the need for a systematic assessment of degradation heterogeneity in LED reliability studies through voltage degradation data from SSADT. This study does not address heterogeneity across different types of LEDs or across varying stress conditions or causes of heterogeneity. Instead, the focus is on the inherent unit heterogeneity observed within a group of LEDs of the same type, tested under identical experimental conditions. The main research gaps have been covered, with the following main contributions:

- An optimised accelerated step-thermal stress test under constant current is conducted to obtain forward-voltage degradation data of LEDs, enabling efficient acquisition of multi-temperature degradation behaviour and reducing the total testing time.
- Empirical Mode Decomposition (EMD) is applied to extract degradation-informative features, with intrinsic mode functions classified using statistical tests to separate noise from meaningful voltage trends.
- Cross-device degradation heterogeneity is assessed using kernel density estimation (KDE) and quantified via Jensen–Shannon divergence (JSD), Wasserstein distance (WD), and Maximum Mean Discrepancy (MMD), enabling a principled evaluation of variability in LED degradation behaviour.

The remainder of this article is organized follows. Section 2 provides the information of tested LEDs, experiment involving the test set up, devices, and test rigs. The basic theory of EDM, KDE and divergence measures is given in Section 3. Section 4 presents the results and discussions. Finally, Section 5 concludes the article.

2. Experimental setup and data acquisition

In this study, an ADT test was conducted on a 10 W/700 lm high-power white LED [35]. The schematic structure, physical dimensions, and technical specifications of the device under test are presented in Figure 1 and Table 1.

In our experiment, temperature was selected as the sole accelerating stress, while other environmental factors were controlled. A three-step thermal stress profile was applied,

consisting of temperature levels $T_1<T_2<T_3$ with corresponding duration's t_1, t_2 and t_3. The first stress level T_1 was fixed at +60 °C, corresponding to the maximum rated operating temperature of the LED (Table 1) and ensuring consistency with the field degradation mechanism. The highest temperature T_3 was set to +80 °C, providing sufficient acceleration while preventing thermal overstress based on the maximum allowable junction temperature of +115 °C [6]. The intermediate level T_2 was assigned as +70 °C. Based on the rated forward current (Table 1), three LED groups (10 samples per group) were tested at drive currents of (i) 1050 mA, (ii) 525 mA, and (iii) 210 mA.

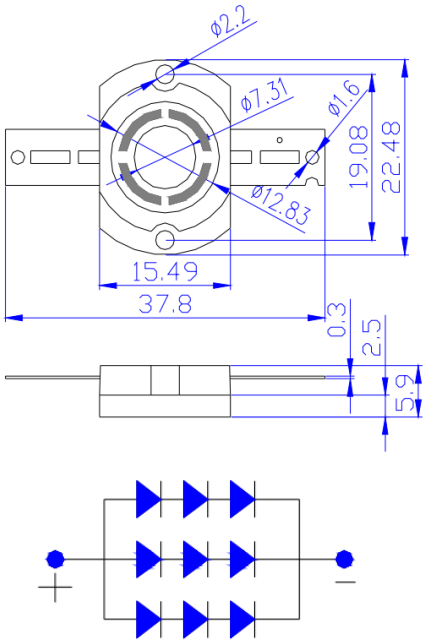

Figure 1. The dimensions of the tested LED GT-P10WW339910700 and its internal circuit diagram [35].

Table 1. The technical characteristics of tested LED [35].

Parameters	Values	Unit
Luminous flux	700	lm
Correlated colour temperature/Wavelength	2900 ~ 3200	K/nm
Forward voltage	9 ~ 11	V
Forward current	1050	mA
Thermal resistance	12	°C/W
Junction temperature	115	°C
Operating temperature	-40 ~ 60	°C

To allocate the optimal durations for the stepwise temperature profile, a simulation-based design optimization framework was employed. The method integrates Monte-Carlo simulation, maximum likelihood estimation (MLE) under right-censoring, and a genetic algorithm to optimize the SSALT plan. This framework follows classical reliability design principles [4,36] and incorporates modern extensions for nonlinear and multi-stress models [37]. The framework offers several advantages over conventional SSALT planning. First, it does not require closed-form Fisher information, which is often unavailable for nonlinear acceleration models or censored step-stress structures. Instead, the statistical precision of the lifetime estimator is evaluated directly through replicated Monte-Carlo analysis, enabling application to any parametric lifetime model. Second, because the objective function is defined as the empirical variance of the log-median lifetime, the optimization targets the true estimation uncertainty rather than analytical approximations. Third, the use of GA provides global search capability, improving robustness in non-convex design spaces. As a result, the optimized plan (i) preserves the underlying failure mechanism, (ii) reduces total testing time, and (iii) enhances extrapolation accuracy under use conditions.

The typical ambient temperature for LED operation is assumed to be +25 °C [38]. The lifetime distribution was modelled using a Weibull distribution with parameters β=14.72 and η=2706.25, referenced from equivalent LED data [34]. The practical service lifetime was set to 30.5360 years (≈269,991 h) [34]. Because the stress involves temperature and drive current, the Arrhenius model and inverse power law [5] were used to establish the life–stress relationship. The optimization objective was to minimize the variance of the log-median lifetime. After optimization, the optimized test durations at +60 °C, +70 °C, and +80 °C were 1113.26, 871.10, and 478.64 hours, respectively. For practical implementation and smoother stress transitions, these durations were adjusted to 1080, 840, and 480 hours, respectively. The final test plan is illustrated in Figure 2.

During the test, a thermal chamber, DC power supplies, data loggers, and a central monitoring computer (see Figure 3) were employed to ensure (i) stable and accurate current supply to each LED, (ii) controlled thermal stress conditions, and (iii) continuous real-time measurement and recording of voltage degradation data. The temperature inside the thermal chamber is stably set and controlled through dedicated software. This temperature is continuously monitored and automatically adjusted to maintain the prescribed thermal conditions. All

LEDs in a group are mounted on a common aluminium plate, which has high thermal conductivity and minimizes the temperature difference between devices. Therefore, the LEDs in a group are subjected to approximately the same effective thermal stress, ensuring that relative differences in degradation behaviour can be evaluated.

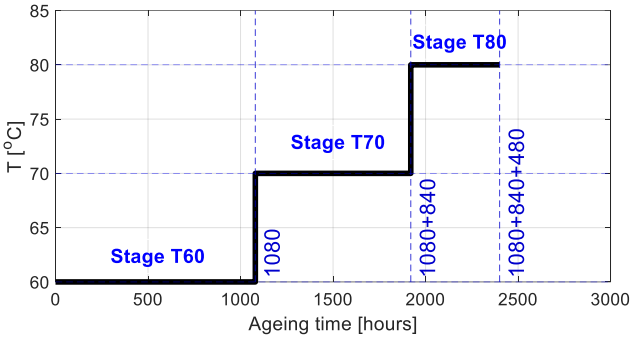

Figure 2. The experimental temperature profile for the ATs of LEDs.

In this experiment, we focused on obtaining the voltage variation of LEDs. The test terminated when the test time set above was reached. Voltage was continuously monitored and recorded every 10 minutes, yielding up to approximately 6400, 5000, and 2800 samples per group corresponding to stress levels +60, +70, and +80 °C, respectively. This acquisition provides high-frequency data and sufficiently long and valuable time series for statistical analysis. The raw voltage data for the three current groups are shown in Figure 4 and Table 2.

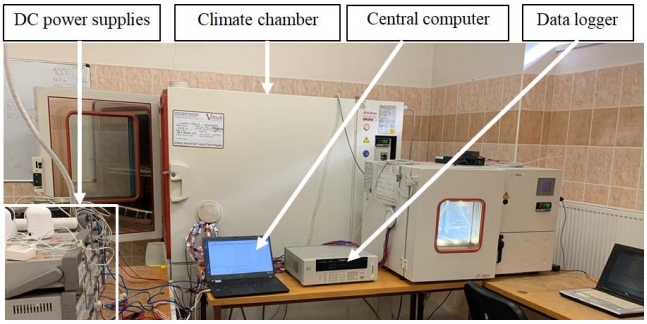

Figure 3. The test rigs of the experiment including thermal climate chamber, DC power supplies, central computer and data logger.

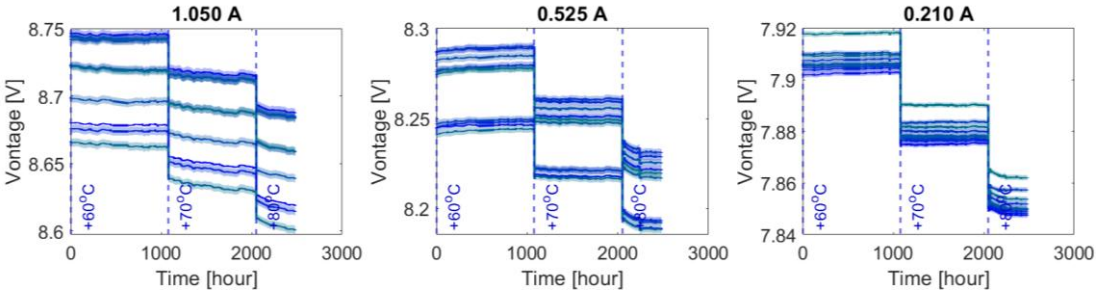

Figure 4. Graphical plots of the raw voltage data of tested LEDs at the current levels of 1050 mA (left), 525 mA (middle) and 210 mA (right) under a step thermal stress AT.

Table 2. An example of the raw voltage data of tested LEDs under a step thermal stress AT.

Time [hour]	**Voltage [V]** (1050 mA)	**Voltage [V]** (525 mA)	**Voltage [V]** (210 mA)
	T = + 60°C		
0	8.746509	8.244681	7.905493
0.16	8.746468	8.24464	7.90555
0.33	8.746386	8.244632	7.905526
...	…	…	…
	T = + 70°C		
1080	8.722047	8.221457	7.879998
1080.16	8.721571	8.220637	7.879325
1080.33	8.721309	8.220276	7.879129
...	…	…	…
	T = + 80°C		
1920	8.69469	8.194896	7.853354
1920.16	8.693624	8.194437	7.852887
1920.33	8.693772	8.19456	7.852887
...	…	…	…

To properly assess the heterogeneity in degradation behaviour, the degradation data were analysed separately for each temperature level and drive-current group. Thermal stress and electrical stress influence LED degradation through different physical mechanisms, temperature accelerates defect generation and material ageing, while higher drive current increases junction temperature via self-heating. When observations across different stress conditions are pooled, the resulting dataset becomes a mixture of trajectories governed by different effective stress levels, obscuring systematic differences in degradation rates, bias statistical inference on the shape and scale of the degradation distribution, and violate key assumptions of accelerated testing. From a modelling perspective, mixing heterogeneous degradation paths leads to distorted estimates of critical parameters: (i) the slope and curvature of the degradation trend, (ii) the variance structure of the data component, and (iii) the parameters of the assumed lifetime distribution. Analysing within each temperature–current subgroup therefore, ensures that degradation dynamics, acceleration factors, and distributional parameters are estimated consistently under homogeneous stress conditions, enabling meaningful comparisons across groups and preserving the physical interpretability of the accelerated test results.

3. Methodology for analysis of LED degradation heterogeneity

Degradation behaviour analysis is a key aspect of LED reliability research. The main task is to address how LEDs degrade under various test conditions and how the resulting variability can be quantified. In reliability studies, the degradation of LEDs can be represented by a common degradation trajectory model, in which the observed degradation signal of each unit is decomposed into a systematic trend component and stochastic deviations reflecting measurement noise and intrinsic variability. Formally, the degradation of the *i*-th LED at time *t* can be expressed as:

$$Y_i(t) = f_i(\boldsymbol{\theta}, t) + \varepsilon_i(t) \quad (1)$$

where $f_i(\boldsymbol{\theta},t)$ denotes the underlying degradation trend, $\boldsymbol{\theta}$ is the set of degradation parameters, and $\varepsilon_i(t)$ captures random fluctuations and intrinsic variability. Intrinsic variability is understood as the inherent fluctuations or differences of the degradation process itself, arising from the material characteristics and operating mechanism of each LED.

In this study, the heterogeneity in the degradation trend $f_i(\boldsymbol{\theta},t)$ is evaluated using the degradation slope, estimated from the main trend extracted via EMD. Meanwhile, heterogeneity in the intrinsic variability is assessed based on the combination of the EMD with KDE and quantifies distributional divergences through JSD, WD, and MMD. This dual-level assessment of heterogeneity in trend and intrinsic variability is crucial. By quantifying the sources of heterogeneity, it provides the information for developing reliable accelerated degradation models and for accurately predicting RUL under varying stress conditions.

3.1. Kernel Density Estimation

Density distribution analysis is a widely used method in data science, and is especially suitable for time series data. KDE method is especially beneficial when the underlying distribution of the data is unknown or uncertain. The KDE is a nonparametric density estimation technique used to estimate the probability density function (PDF) of a random variable [39].

For a given dataset $\boldsymbol{Y} = (Y_1, Y_2, \ldots, Y_m)$, the estimated density at an observation point *y* is computed as the average of kernels centred at each sample point, and is mathematically defined as:

$$\hat{f}(y) = m^{-1}h^{-1}\sum_{i=1}^{m} K\left(\frac{y-Y_i}{h}\right), -\infty < y < +\infty \quad (2)$$

where $\hat{f}(y)$denotes the estimated density at point *y*; *m* is the number of observations of **Y**; *h* is the bandwidth parameter that controls the smoothness of the density estimation; $K(\bullet)$ is the kernel function, which is typically a symmetric PDF; and Y_i represents each data point in the sample.

In KDE, two key considerations are the choice of kernel function and the selection of bandwidth. The classical kernel estimation can be found in [40]. The kernel determines how data around each observation is smoothed, with the Gaussian kernel being widely used due to its smoothness and theoretical foundation. However, prior study [39] emphasise that the bandwidth plays a more critical role, as it directly controls the smoothness of the estimated density. Several methods exist for bandwidth selection, including rule-of-thumb approaches, cross-validation, and the Sheather–Jones (SJ) method. Among these, the SJ method for estimating bandwidth in KDE [41] is particularly favoured for its accuracy and stability across a wide range of distributions, making it the default choice in many statistical applications. This method is proposed to select

bandwidth by minimizing the approximate mean square integral error:

$$AMISE(h) = \frac{R(K)}{nh} + \frac{1}{4}\mu_2(K)^2 h^4 R(f") \quad (3)$$

where

$$R(K) = \int_{-\infty}^{+\infty} K(u)^2 du, \mu_2(K) = \int u^2 K(u) du \quad (4)$$

and

$$R(f") = \int \left(f"(y)\right)^2 dy \quad (5)$$

The theoretical optimal bandwidth is then determined by:

$$h^* = \left(\frac{R(K)}{\mu_2(K)^2 R(f") n}\right)^{1/5} \quad (6)$$

Since $R(f")$ is unknown, SJ uses the estimation plug-in: estimates $f"$ through KDE with pilot bandwidth, then substitutes it into the above formula. The result is a nonlinear equation that needs to be solved numerically to get the optimal bandwidth.

3.2. Empirical Mode Decomposition

Feature extraction transforms complex raw data into concise, meaningful representations by reducing noise and dimensionality, thereby improving modelling, prediction, and classification performance. EMD method, proposed by Huang et al. [42], decomposes a nonlinear and no stationary signal into a set of Intrinsic Mode Functions (IMFs) and a residual, as presented in Equation (7). Each IMF captures oscillations at a specific time scale, revealing the underlying dynamical structure without prior assumptions on stationary or functional form. Unlike traditional methods such as Fourier or Wavelet Transform, EMD is fully adaptive and data-driven, making it particularly effective for analysing nonlinear, non-standard, and time-varying signals. An IMF is defined by two conditions: (1) the number of zero crossings and extrema differ at most by one, and (2) the mean of the upper and lower envelopes is zero at all times [43].

$$Y(t) = \sum_{i=1}^{n} IMF_i(t) + r(t) \quad (7)$$

where $Y(t)$ is obtained time-domain data, $IMF_i(t)$ is the ith IMF, n is the number of IMFs, extracted from original data and $r(t)$ is residual data, which is main trend of $Y(t)$. The main process of the EDM for degradation data of equipment in each stage is summarized below:

- Initialize the degradation data $Y(t)$
- Find the upper and lower extrema e_{upper}, e_{lower} points of Y and calculate the mean of upper and lower envelopes using p-chip interpolation:

$$I(t) = Y(t) - \frac{e_{upper} + e_{lower}}{2} \quad (8)$$

$I(t)$ is the 1st IMF if two conditions are satisfied, if not the step (2) are repeated until two conditions are met and $I(t)$ is regarded the 1st IMF.

- Calculate $r(t) = Y(t) - IMF_1(t)$, and set $r(t)$ as the new $Y(t)$.
- Repeat the step (2), (3) until $r(t)$ becomes a monotonic function.

By using the EMD, the LED degradation data are decomposed into multiple IMFs and residual components. In the composite degradation trajectory, the residual component is regarded as the main degradation trend [44], while the IMFs capture different layers of intrinsic variability superimposed on the main degradation trend. High-frequency IMFs generally reflect measurement noise or rapid fluctuations, while lower-frequency IMFs reflect slower variations [42] that are not part of the long-term trend and are treated as representations of intrinsic variability, capturing local oscillations and micro-fluctuations in the degradation process. By isolating these components, the IMFs help quantify the within-path variability and clarify the heterogeneity in degradation behaviour across LEDs, allowing the degradation process to be analysed more reliably.

3.3. Quantification of distributional divergences

Quantifying divergences between distributions is an important step in data analysis, helping to assess the variability and heterogeneity between data sets that traditional summary statistics such as mean or variance do not adequately capture. In the context of degradation data analysis, comparing distributions of different samples allows for the identification of unusual samples and the assessment of uniformity during degradation.

Let (X, B) be a measurable space, where X is the sample space and B is a σ-algebra on X. Given observed data $Y_1, Y_2, \ldots, Y_N$ are random variables defined on X with the respective independently and identically distributed (i.i.d.) $\{P1, P2, \ldots, PN\} \in P(X)$ defined on (X, B). For any two probability distributions P_i, P_j, a divergence measure is a nonnegative

functional:

$$D(P_i, P_j): P(X) \times P(X) \to R_{\geq 0} \quad (9)$$

Such that $D(P_i, P_j) = 0 \Leftrightarrow P_i = P_j$

Given the collection of N probability distributions $\{P_1, P_2, .., P_N\}$, the global heterogeneity index is the empirical mean of pairwise divergences is given:

$$H_D(\{P_1, P_2, \ldots, P_N\}) = E_{(I,J)}[D(P_I, P_J)] \quad (10)$$

where the expectation is taken with respect to the uniform distribution over unordered pairs $(I, J), I \neq J$.

Let $\Omega = \{(i, j): 1 \leq i \leq j \leq N\}$. The number of such unordered pairs is $|\Omega| = \frac{N(N-1)}{2}$. The empirical mean of pairwise divergences is computed by definition of uniform expectation:

$$E_{(I,J)}[D(P_I, P_J)] = \frac{1}{|\Omega|} \sum_{(i,j)\in\Omega} D(P_i, P_j) \quad (11)$$

Substituting $|\Omega| = \frac{N(N-1)}{2}$ gives:

$$E_{(I,J)}[D(P_I, P_J)] = \frac{2}{N(N-1)} \sum_{(i,j)\in\Omega} D(P_i, P_j) \quad (12)$$

Therefore, the global heterogeneity index associated with $D(\cdot)$ is defined as the average pairwise divergence:

$$H_D(\{P_1, P_2, \ldots, P_N\}) = \frac{2}{N(N-1)} \sum_{1\leq i\leq j\leq N} D(P_i, P_j) \quad (13)$$

The index quantifies the global dispersion or dissimilarity of the family $\{P_1, P_2, .., P_N\}$ in the divergence-induced geometry. For a single distribution P_i, a local heterogeneity index related to P_i can be defined by:

$$H_D(P_i|\{P_1, P_2, \ldots, P_N\}) = \frac{1}{N-1} \sum_{\substack{j=1 \\ j\neq i}}^{N} D(P_i, P_j) \quad (14)$$

which measures the average divergence between P_i and all other distribution. Both global and local indices can be used to quantify distributional heterogeneity in multi-sample or federated learning contexts. In the multi-scale case, suppose that at "scale" m each device i gives a distribution $P_{i,m}$. We define the heterogeneity index at scale m:

$$H_D^{(m)} = \frac{2}{N(N-1)} \sum_{0\leq i\leq j\leq N} D(P_{i,m}, P_{j,m}) \quad (15)$$

Therefore, the composite multi-scale index is defined by:

$$H_D = \sum_{m=1}^{M} w_m H_D^{(m)} \quad (16)$$

where w_k is weighted by the importance of the scale.

In this study, JSD, WD, and MMD were employed as quantitative measures of divergence to assess heterogeneity in LED degradation across different temperature and drive-current groups. Meanwhile, the Kullback–Leibler divergence (KLD) is often insensitive to tail differences [45] and may be undefined when the distributions have non-overlapping support. Parametric tests such as the chi-square test rely on restrictive assumptions (e.g., sample-size requirements, independence) [46] that are rarely satisfied in degradation data. Likewise, the Kolmogorov–Smirnov test shows low sensitivity to differences in higher-order moments or tail behaviour [47]. The JSD is a symmetric, bounded measure derived from the KLD. It quantifies the similarity between probability distributions in a way that is robust to zero-probability bins, making it suitable for discrete or histogram-based representations of degradation signals [48]. The WD, also known as the Earth Mover's Distance, evaluates the minimal "effort" required to transform one distribution into another, incorporating the geometry of the support space. The WD is particularly advantageous when the distributions exhibit shifts or scale differences [49]. The MMD is a kernel-based measure that captures higher-order differences between distributions, including differences in moments and shapes, and is well-suited for non-parametric settings where the distributions may not follow standard theoretical forms [50].

By combining these three measures, the study leverages a multi-faceted evaluation of divergence: JSD captures overall probabilistic similarity, the WD emphasizes the geometric or structural difference, and the MMD detects subtle differences in higher-order statistics. This integrated approach ensures a robust assessment of heterogeneity in LED degradation, accounting for variations in both central tendency and distributional shape across stress groups.

The JSD is a symmetric and differentiable measure for comparing the differences between two probability distributions, built on the KLD but overcomes the disadvantages such as: being asymmetric and possibly infinite when the two distributions do not have the same support. For any two probability distributions P_i, P_j, the JSD is defined by [48]:

$$D_{JS}(P_i \| P_j) = \frac{1}{2} D_{KL}(P_i \| M_{ij}) + \frac{1}{2} D_{KL}(P_j \| M_{ij}) \quad (17)$$

where $M_{ij} = \frac{1}{2}(P_i + P_j)$ is mixture probability of P_i, P_j; and $D_{KL}(P_i \| P_j) = \sum_k p_{ik} \, log \frac{p_{ik}}{p_{jk}}$ is the KLD.

The JSD can be represented in detail as:

$$D_{JS}(P_i \| P_j) = \frac{1}{2}\sum_{y\in X} P_i(x)\, log\, \frac{P_i(y)}{M_{ij}(y)} + \frac{1}{2}\sum_{x\in X} P_j(y)\, log\, \frac{P_j(y)}{M_{ij}(y)} \quad (18)$$

Meanwhile, the WD measures the "minimum cost" of transforming a distribution P_i into a distribution P_j, where cost is understood as "mass × distance travelled". In other words, it describes the minimum amount of work needed to "move the soil" (probability mass) from shape P_i to shape P_j. WD order p ($p \geq 1$) is defined by [49]:

$$W_p(P_i, P_j) = \left(\inf_{\gamma\in\Gamma(P_i,P_j)} \int_{X\times X} d(x,y)^p d\gamma(x,y) \right)^{\frac{1}{p}} \quad (19)$$

The first order WD:

$$W_1(P_i, P_j) = \inf_{\gamma\in\Gamma(P_i,P_j)} \int_{X\times X} d(x,y) d\gamma(x,y) \quad (20)$$

where $\Gamma(P_i, P_j)$ is the set of joint distribution which marginal distributions are P_i, P_j, $d(x, y)$ is the Euclidean distance, and $\gamma(x, y)$ is the method to distribute mass to convert P_i to P_j.

In another approach, the MMD is a widely used non-parametric distance measure for comparing two probability distributions. The core idea of the MMD is to map data from the observation space to the Recurrent Hilbert Space through a feature kernel, and then measure the distance between the mean vectors in this space. Because it does not require any assumptions about the distribution shape and is scalable to high-dimensional data, the MMD has been applied in many fields such as non-parametric hypothesis testing, generative anomaly modelling evaluation, domain adaptation, and degenerative data analysis to determine the homogeneity of samples. MMD^2 between any two distributions P_i, P_j, is defined by [50]:

$$MMD^2(P_i, P_j) = \left\| E_{X_i\sim P_i}[\phi(Y_i)] - E_{X_j\sim P_j}[\phi(Y_j)] \right\|_H^2 \quad (21)$$

$$MMD^2(P_j, P_j) = \left\| \mu_{P_i} - \mu_{P_j} \right\|_H^2, \mu_{P_i} := E_{X_i\sim P_i}[\phi(Y_i)] \in H \quad (22)$$

where ϕ is the feature mapping defined by the kernel $k(Y_i, Y_j) = \langle \phi(Y_i), \phi(Y_j) \rangle$. The biased estimator of MMD^2 is defined by:

$$MMD^2(\hat{P}_i, \hat{P}_j) = \frac{1}{n_i^2}\sum_a \sum_b k(y_{ia}, y_{ib}) + \frac{1}{n_j^2}\sum_a \sum_b k(y_{ja}, y_{jb}) - \frac{2}{n_i n_j}\sum_a \sum_b k(y_{ia}, y_{jb}) \quad (23)$$

4. Results and discussion

In this study, the high-frequency voltage data were used directly for EMD without down-sampling or explicit noise filtering. The adaptive nature of EMD allows the decomposition of non-linear and non-stationary signals IMFs, which separate high-frequency components, often corresponding to measurement noise or transient fluctuations, from lower-frequency modes that reflect the underlying degradation dynamics. The combination of high-resolution data and EMD facilitates both precise extraction of degradation trends and comparative statistical evaluation across stress conditions, improving the interpretability and reliability of accelerated degradation analyses. In this section, the evaluation results of LED degradation heterogeneity are presented. The analysis is performed for LEDs under identical test conditions and operating modes. We perform the analysis on two main aspects: i) analysis of degradation heterogeneity and ii) testing of the homogeneity hypothesis. The KDE method is applied with a Gaussian kernel, and the bandwidth is optimized using the SJ plug-in method [41]. In addition, the MMD measure is used with a Gaussian kernel, in which the bandwidth is determined using the median heuristic method [51]. The weights of the IMFs are determined based on their energy levels.

4.1. Analysis of degradation heterogeneity of LEDs

To analyse heterogeneity in the LED degradation process, the degradation data of LEDs were first grouped according to their temperature and drive-current conditions to ensure that each dataset represented a homogeneous degradation mechanism, as mentioned in Section 2. The grouped degradation data were then decomposed into a main degradation trend and a set of oscillatory components using EMD, forming the composite degradation trajectory. Figure 5 illustrates the first five IMFs of LED 1 operated at 1050 mA and +60 °C as an example.

In practice, measurement data are inevitably contaminated by white noise, and thus not all IMFs obtained from EMD decomposition are meaningful. To separate voltage degradation

trend from high-frequency noise or transient fluctuations, we applied a multi-criteria IMF selection and denoising procedure following EMD. As EMD is fully data-adaptive, initial high-frequency IMFs may be noise-dominated, necessitating robust filtering. First, each IMF was subjected to a Ljung–Box Q-test [52], and those failing to reject the white-noise hypothesis at 5% significance were excluded, preventing residual noise from contaminating the degradation trend [42,53]. Surviving IMFs were further filtered based on relative energy (<5% of total) and high-frequency content, following established EMD denoising practices [54]. Finally, monotonicity was assessed using the Mann–Kendall trend test [55,56] or linear regression slope analysis [57], retaining only IMFs with statistically significant trends ($p < 0.05$) and slope magnitudes above 5% of the IMF margin, ensuring that oscillatory or quasi-periodic components are not misinterpreted as long-term degradation. Figure 6 illustrates the time series, autocorrelation, histogram, and power spectrum of an example IMF, providing evidence for the IMF classification procedure. This hybrid approach, combining EMD with statistical tests and energy/frequency-based thresholding, offers several advantages: it reduces spurious high-frequency noise and mode-mixing artefacts, preserves components that reliably represent the underlying degradation, and allows threshold validation via sensitivity analysis to ensure reproducibility. After filtering, the "denoised" degradation signal was reconstructed by summing only the retained IMFs and the residual component.

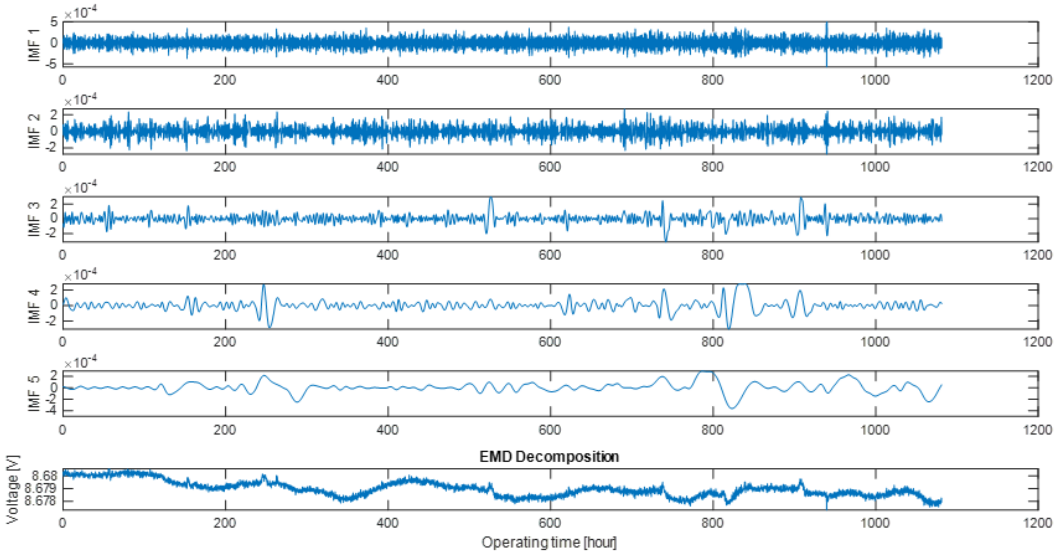

Figure 5. Illustration of EMD of degradation voltage data of LED1 under temperature of +60 ℃ at current of 1050 mA.

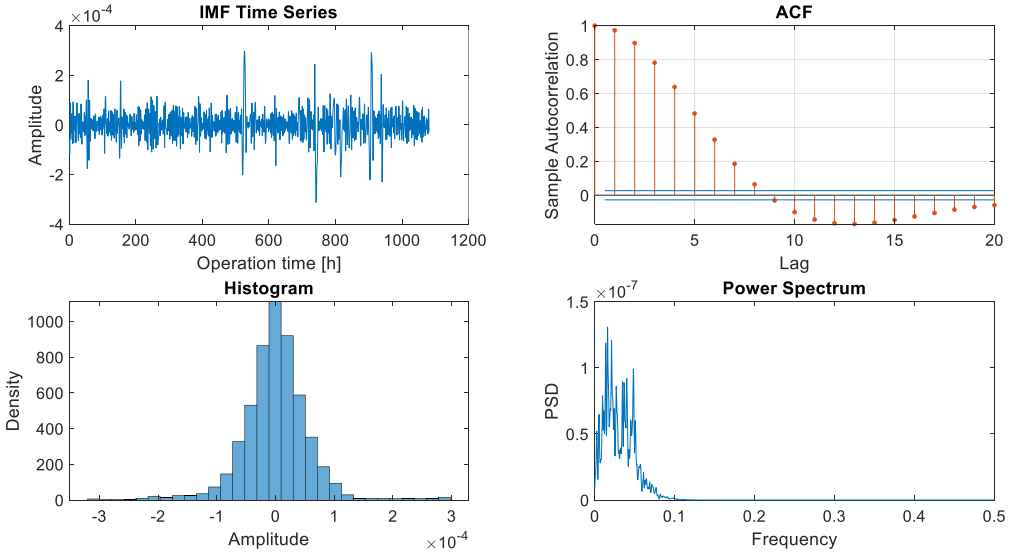

Figure 6. Illustration of time series, autocorrelation function, histogram, power spectrum plots of an IMF.

To ensure the rigour and representativeness of the extracted degradation trend, the residual component was subjected to the same testing procedure as described above, followed by a dedicated monotonicity assessment. Monotonicity was evaluated by computing the first-order differences between consecutive samples, $\Delta r(t_i) = r(t_{i+1}) - r(t_i)$. This criterion ensures that the residual indeed represents a meaningful, slowly varying trajectory suitable for subsequent statistical modelling of the degradation process. A residual path was considered effectively monotonic if the vast majority of $\Delta r(t_i)$ values shared the same sign. Visual inspection and statistical evaluation both confirmed the absence of oscillatory behaviour incompatible with an underlying degradation trend. Thereby, this residual component is regarded as the main degradation trend. The IMFs capture different layers of intrinsic variability superimposed on this main degradation trend.

In this study, degradation heterogeneity is examined from two complementary perspectives: (i) heterogeneity in the main degradation trends, which reflects differences in initial degradation levels and long-term degradation rates; and (ii) heterogeneity in the oscillatory components (IMFs), which represent fluctuations around the trend and capture intrinsic variability within the degradation process.

Figure 7 shows the adjusted main degradation trends, of LEDs operated at 1050 mA (top), 525 mA (middle), and 210 mA (bottom). These trends are normalised by subtracting their initial degradation values so that all trajectories start at zero, thereby allowing a clearer visual comparison of their degradation slopes. Tables 3–5 report the initial degradation values and degradation slopes derived from the EMD-extracted residuals. The slopes were estimated using MLE to ensure statistical efficiency and robustness. Table 6 provides the average junction temperature difference of the LEDs between different thermal stresses determined based on the slope of the degradation curve and the Arrhenius [5]. As shown in Figure 8 and Tables 3-5, LED degradation heterogeneity manifests in two complementary dimensions: (1) absolute degradation levels (differences in initial voltage values), and (2) degradation kinetics (differences in slope). The results reported in Table 6 confirms that the estimated junction temperature differences closely align with the temperature steps applied in the tests, demonstrating that the degradation slopes reliably reflect the actual thermal stress conditions.

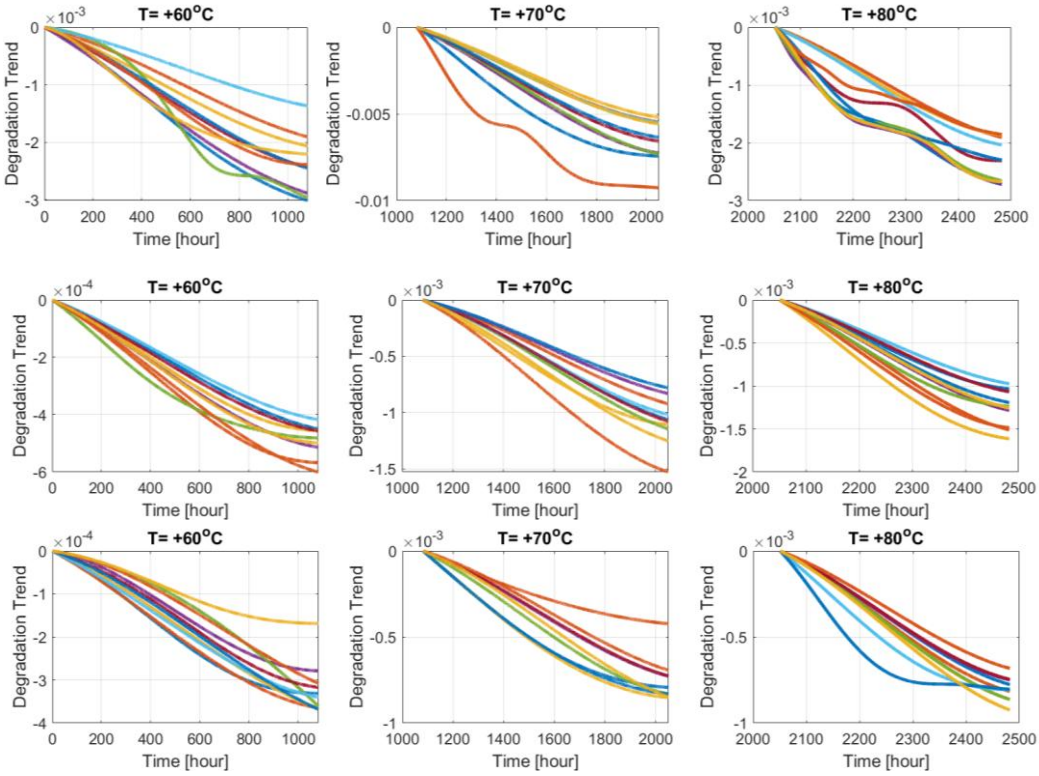

Figure 7. The graphical plots of the adjusted degradation trends from EMD analysis of LEDs at the current level of 1050 mA (top), 525 mA (middle) and 210 mA (bottom).

Table 3. The initial degradation values and slope of degradation trend of LED at current level of 1050 mA.

LED-ID	T = +60 °C		T = +70 °C		T = +80 °C	
	Initial voltage [V]	*Drift* [V/h]	*Initial voltage* [V]	*Drift* [V/h]	*Initial voltage* [V]	*Drift* [V/h]
1	8.679766	$-3.33\cdot10^{-6}$	8.654863	$-7.66\cdot10^{-6}$	8.627157	$-1.89\cdot10^{-5}$
2	8.745670	$-2.10\cdot10^{-6}$	8.719252	$-5.64\cdot10^{-6}$	8.692112	$-1.33\cdot10^{-5}$
3	8.743251	$-2.28\cdot10^{-6}$	8.715490	$-5.36\cdot10^{-6}$	8.688151	$-1.30\cdot10^{-5}$
4	8.675236	$-3.19\cdot10^{-6}$	8.650314	$-7.49\cdot10^{-6}$	8.623475	$-1.89\cdot10^{-5}$
5	8.721904	$-3.27\cdot10^{-6}$	8.693562	$-7.56\cdot10^{-6}$	8.666620	$-1.85\cdot10^{-5}$
6	8.741322	$-2.27\cdot10^{-6}$	8.715616	$-5.66\cdot10^{-6}$	8.688586	$-1.42\cdot10^{-5}$
7	8.697613	$-2.68\cdot10^{-6}$	8.671483	$-6.78\cdot10^{-6}$	8.645520	$-1.61\cdot10^{-5}$
8	8.742674	$-2.07\cdot10^{-7}$	8.715497	$-6.55\cdot10^{-6}$	8.689359	$-1.60\cdot10^{-5}$
9	8.665605	$-2.64\cdot10^{-6}$	8.639678	$-6.37\cdot10^{-6}$	8.610254	$-1.68\cdot10^{-5}$
10	8.721637	$-2.44\cdot10^{-6}$	8.693179	$-5.75\cdot10^{-6}$	8.667198	$-1.43\cdot10^{-5}$

Table 4. The initial degradation values and slope of degradation trend of LED at current level of 525 mA.

LED-ID	T = +60 °C		T = +70 °C		T = +80 °C	
	Initial voltage [V]	*Drift* [V/h]	*Initial voltage* [V]	*Drift* [V/h]	*Initial voltage* [V]	*Drift* [V/h]
11	8.244681	$-4.97\cdot10^{-7}$	8.221457	$-1.11\cdot10^{-6}$	8.192814	$-2.40\cdot10^{-6}$
12	8.275884	$-6.25\cdot10^{-7}$	8.254341	$-1.43\cdot10^{-6}$	8.225152	$-3.50\cdot10^{-6}$
13	8.244878	$-5.05\cdot10^{-7}$	8.224604	$-1.14\cdot10^{-6}$	8.197039	$-2.60\cdot10^{-6}$
14	8.287069	$-5.70\cdot10^{-7}$	8.262460	$-1.29\cdot10^{-6}$	8.232587	$-2.98\cdot10^{-6}$
15	8.286594	$-5.30\cdot10^{-7}$	8.263626	$-1.18\cdot10^{-6}$	8.236210	$-2.87\cdot10^{-6}$
16	8.246887	$-4.59\cdot10^{-7}$	8.224983	$-1.05\cdot10^{-6}$	8.195997	$-2.26\cdot10^{-6}$
17	8.282296	$-5.55\cdot10^{-7}$	8.258310	$-1.11\cdot10^{-6}$	8.229401	$-2.48\cdot10^{-6}$
18	8.276884	$-5.52\cdot10^{-7}$	8.250610	$-1.21\cdot10^{-6}$	8.220710	$-2.76\cdot10^{-6}$
19	8.240925	$-6.60\cdot10^{-7}$	8.220424	$-1.58\cdot10^{-6}$	8.192204	$-3.44\cdot10^{-6}$
20	8.274162	$-5.05\cdot10^{-7}$	8.252952	$-1.29\cdot10^{-6}$	8.223991	$-2.91\cdot10^{-6}$

Table 5. The initial degradation values and slope of degradation trend of LED at current level of 210 mA.

LED-ID	T = +60 °C		T = +70 °C		T = +80 °C	
	Initial voltage [V]	*Drift* [V/h]	*Initial voltage* [V]	*Drift* [V/h]	*Initial voltage* [V]	*Drift* [V/h]
21	7.905493	$-3.65\cdot10^{-7}$	7.87970	$-8.18\cdot10^{-7}$	7.851761	$-1.80\cdot10^{-6}$
22	7.901959	$-4.03\cdot10^{-7}$	7.87654	$-8.73\cdot10^{-7}$	7.849277	$-1.89\cdot10^{-6}$
23	7.903845	$-4.04\cdot10^{-7}$	7.87805	$-8.79\cdot10^{-7}$	7.850245	$-2.01\cdot10^{-6}$
24	7.904837	$-3.31\cdot10^{-7}$	7.87893	$-7.51\cdot10^{-7}$	7.850680	$-1.74\cdot10^{-6}$
25	7.907469	$-4.01\cdot10^{-7}$	7.88178	$-8.58\cdot10^{-7}$	7.853968	$-2.01\cdot10^{-6}$
26	7.909987	$-3.75\cdot10^{-7}$	7.88486	$-7.83\cdot10^{-7}$	7.857737	$-1.87\cdot10^{-6}$
27	7.906010	$-3.52\cdot10^{-7}$	7.88006	$-7.50\cdot10^{-7}$	7.851834	$-1.73\cdot10^{-6}$
28	7.905747	$-4.07\cdot10^{-7}$	7.87941	$-8.58\cdot10^{-7}$	7.852589	$-2.05\cdot10^{-6}$
29	7.909454	$-3.40\cdot10^{-7}$	7.88331	$-7.16\cdot10^{-7}$	7.855621	$-1.58\cdot10^{-6}$
30	7.917753	$-4.20\cdot10^{-7}$	7.89198	$-8.76\cdot10^{-7}$	7.863932	$-2.14\cdot10^{-6}$

To further analyse heterogeneity, it is essential to examine the distributional characteristics of the individual IMFs that compose composite degradation trajectory. Variations in amplitude, shape, or kinetics of the IMFs across LEDs can reveal whether heterogeneity arises from local fluctuations or from systematic differences in the degradation mechanism. Accounting for IMF-level distributional heterogeneity thus strengthens the robustness of reliability models and enhances confidence in accelerated lifetime testing and predictive analyses. To quantify this heterogeneity, global (GHI) and local heterogeneity indices (LHI) were computed from pairwise divergences using formulas (11), (12), and (14), derived from the IMFs and their KDEs. Two complementary analyses were

performed: (i) a distribution shape-only assessment using normalised IMFs, which isolates distribution-shape differences, and (ii) a raw-distribution assessment using unnormalized IMFs, which captures differences in mean, variance, and shape. Comparing the two sets of indices helps identify the dominant source of variability: larger discrepancies in the raw-distribution indices indicate heterogeneity driven mainly by degradation magnitude, whereas larger discrepancies in the distribution shape-only indices reflect differences in shape and degradation kinetics.

Table 6. The average junction temperature difference of the LEDs between different thermal stresses.

LED-ID	**1050 mA**		**LED-ID**	**525 mA**		**LED-ID**	**210 mA**	
	60 ℃-70 ℃	70 ℃-80 ℃		60 ℃-70 ℃	70 ℃-80 ℃		60 ℃-70 ℃	70 ℃-80 ℃
1	12.04	13.04	11	11.41	11.29	21	11.64	11.38
2	14.24	12.35	12	11.94	12.92	22	11.16	11.16
3	12.34	12.79	13	11.77	11.86	23	11.23	11.87
4	12.34	13.32	14	11.75	12.10	24	11.82	12.12
5	12.09	12.90	15	11.59	12.76	25	11.01	12.22
6	13.22	13.23	16	11.95	11.03	26	10.61	12.56
7	13.38	12.43	17	11.38	11.58	27	10.93	12.06
8	12.76	12.87	18	11.31	11.92	28	10.76	12.56
9	12.72	13.98	19	12.56	11.27	29	10.75	11.44
10	12.40	13.12	20	12.33	11.73	30	10.61	12.90

To further analyse heterogeneity, it is essential to examine the distributional characteristics of the individual IMFs that compose composite degradation trajectory. Variations in amplitude, shape, or kinetics of the IMFs across LEDs can reveal whether heterogeneity arises from local fluctuations or from systematic differences in the degradation mechanism. Accounting for IMF-level distributional heterogeneity thus strengthens the robustness of reliability models and enhances confidence in accelerated lifetime testing and predictive analyses. To quantify this heterogeneity, global (GHI) and local heterogeneity indices (LHI) were computed from pairwise divergences using formulas (11), (12), and (14), derived from the IMFs and their KDEs. Two complementary analyses were performed: (i) a distribution shape-only assessment using normalised IMFs, which isolates distribution-shape differences, and (ii) a raw-distribution assessment using unnormalized IMFs, which captures differences in mean, variance, and shape. Comparing the two sets of indices helps identify the dominant source of variability: larger discrepancies in the raw-distribution indices indicate heterogeneity driven mainly by degradation magnitude, whereas larger discrepancies in the distribution shape-only indices reflect differences in shape and degradation kinetics.

Tables 7-9 present the computed GHI and LHI and highlight LED pairwise comparisons whose dispersion exceeds the 2σ threshold of global heterogeneity, based on the classified IMFs. In these tables, lowercase values correspond to distribution shape-only indices, whereas bold values represent raw distribution indices incorporating amplitude and variance. Overall, most LEDs within each group exhibit consistent degradation trends, although some units show deviations. The observed divergence tends to decrease with increasing temperature and/or decreasing current (Figure 8).

A more detailed examination reveals that, at a drive current of 1050 mA, heterogeneity is predominantly governed by amplitude differences across temperatures (Table 7). For LEDs operating at 525 mA, early-stage heterogeneity is mainly amplitude-driven, whereas later-stage differences reflect variations in shape and degradation kinetics (Table 8). At the lowest current level of 210 mA, heterogeneity is consistently dominated by shape and kinetics throughout the degradation process (Table 9). These results indicate a clear dependence of heterogeneity on operating conditions: at high currents and low temperatures, differences in degradation magnitude dominate, while at low currents and high temperatures, variations in the distribution shape and kinetics become the primary source of heterogeneity. Collectively, the GHI and LHI analyses provide quantitative evidence that the nature of LED degradation heterogeneity shifts from amplitude-driven to shape/kinetics-driven as operating stress decreases, highlighting the importance of considering both global and local heterogeneity in reliability assessment.

Table 7. The heterogeneity indices of LEDs at the current level of 1050 mA.

LED-ID	T= +60 ℃			T= +70 ℃			T= +80 ℃		
	JSD	*WD*	MMD^2	*JSD*	*WD*	MMD^2	*JSD*	*WD*	MMD^2
Global index	0.0137(*)	0.0068	0.0024	0.0171	0.0073	0.0043	0.0141	0.0084	0.0027
	0.0169(**)	**0.0127**	**0.0056**	**0.0173**	**0.0110**	**0.0051**	**0.0156**	**0.0132**	**0.0042**
Local index									
1	0.0119	0.0056	0.0015	0.0208	0.0084	0.0075	0.0110	0.0066	0.0021
	0.0160	**0.0135**	**0.0078**	**0.0178**	**0.0115**	**0.0051**	**0.0139**	**0.0133**	**0.0048**
2	0.0122	0.0064	0.0026	0.0146	0.0058	0.0029	0.0131	0.0086	0.0025
	0.0129	**0.0105**	**0.0037**	**0.0128**	**0.0080**	**0.0029**	**0.0133**	**0.0117**	**0.0035**
3	0.0134	0.0065	0.0025	0.0197	0.0079	0.0065	0.0120	0.0073	0.0020
	0.0146	**0.0094**	**0.0031**	**0.0149**	**0.0084**	**0.0032**	**0.0137**	**0.0105**	**0.0027**
4	0.0126	0.0057	0.0020	0.0142	0.0059	0.0031	0.0129	0.0078	0.0028
	0.0142	**0.0112**	**0.0049**	**0.0139**	**0.0088**	**0.0040**	**0.0133**	**0.0108**	**0.0029**
5	0.0126	0.0062	0.0019	0.0154	0.0061	0.0032	0.0118	0.0069	0.0020
	0.0161	**0.0116**	**0.0045**	**0.0170**	**0.0099**	**0.0051**	**0.0133**	**0.0105**	**0.0030**
6	0.0118	0.0063	0.0020	0.0153	0.0072	0.0039	0.0155	0.0087	0.0036
	0.0160	**0.0133**	**0.0067**	**0.0178**	**0.0120**	**0.0068**	**0.0163**	**0.0135**	**0.0044**
7	0.0120	0.0056	0.0015	0.0142	0.0060	0.0033	0.0124	0.0066	0.0018
	0.0193	**0.0128**	**0.0059**	**0.0179**	**0.0116**	**0.0066**	**0.0150**	**0.0123**	**0.0039**
8	0.0125	0.0062	0.0022	0.0139	0.0058	0.0027	0.0126	0.0070	0.0022
	0.0153	**0.0118**	**0.0064**	**0.0151**	**0.0100**	**0.0049**	**0.0139**	**0.0112**	**0.0043**
9	0.0129	0.0062	0.0026	0.0135	0.0066	0.0030	0.0135	0.0085	0.0028
	0.0130	**0.0095**	**0.0029**	**0.0135**	**0.0081**	**0.0029**	**0.0130**	**0.0101**	**0.0028**
10	0.0120	0.0063	0.0024	0.0120	0.0061	0.0025	0.0121	0.0074	0.0025
	0.0149	**0.0108**	**0.0042**	**0.0148**	**0.0103**	**0.0047**	**0.0149**	**0.0153**	**0.0053**
Outliers		2,9			1,2,3			2,3,4,6,9	
		1,5,6,7,8			**1,5,6,7**			**1,2,7,8,10**	

(*) Distribution shape-only indices, (**) Raw distribution indices

Table 8**.** The heterogeneity indices of LEDs at the current level of 525 mA.

LED-ID	T= +60 ℃			T= +70 ℃			T= +80 ℃		
	JSD	*WD*	MMD^2	*JSD*	*WD*	MMD^2	*JSD*	*WD*	MMD^2
Global index	0.0129(*)	0.0072	0.0026	0.0136	0.0044	0.0029	0.0210	0.0060	0.0049
	0.0178(**)	**0.0121**	**0.0065**	**0.0144**	**0.0063**	**0.0035**	**0.0203**	**0.0067**	**0.0042**
Local index									
11	0.0115	0.0070	0.0027	0.0112	0.0038	0.0022	0.0179	0.0054	0.0044
	0.0152	**0.0108**	**0.0063**	**0.0114**	**0.0050**	**0.0026**	**0.0176**	**0.0058**	**0.0045**
12	0.0124	0.0063	0.0025	0.0116	0.0041	0.0021	0.0185	0.0050	0.0045
	0.0157	**0.0107**	**0.0053**	**0.0133**	**0.0058**	**0.0032**	**0.0158**	**0.0051**	**0.0033**
13	0.0109	0.0070	0.0022	0.0139	0.0047	0.0032	0.0170	0.0051	0.0036
	0.0140	**0.0119**	**0.0048**	**0.0129**	**0.0059**	**0.0028**	**0.0160**	**0.0058**	**0.0030**
14	0.0115	0.0064	0.0025	0.0124	0.0035	0.0028	0.0203	0.0056	0.0045
	0.0139	**0.0097**	**0.0047**	**0.0130**	**0.0052**	**0.0028**	**0.0186**	**0.0068**	**0.0032**
15	0.0124	0.0065	0.0025	0.0129	0.0038	0.0031	0.0208	0.0055	0.0055
	0.0168	**0.0104**	**0.0061**	**0.0120**	**0.0053**	**0.0027**	**0.0168**	**0.0054**	**0.0026**
16	0.0106	0.0059	0.0020	0.0135	0.0042	0.0035	0.0199	0.0059	0.0052
	0.0160	**0.0101**	**0.0059**	**0.0131**	**0.0058**	**0.0032**	**0.0183**	**0.0058**	**0.0036**
17	0.0106	0.0060	0.0020	0.0126	0.0039	0.0029	0.0162	0.0047	0.0035
	0.0168	**0.0112**	**0.0066**	**0.0136**	**0.0059**	**0.0038**	**0.0161**	**0.0053**	**0.0031**
18	0.0099	0.0053	0.0014	0.0105	0.0036	0.0016	0.0252	0.0063	0.0064
	0.0154	**0.0106**	**0.0053**	**0.0118**	**0.0050**	**0.0024**	**0.0252**	**0.0068**	**0.0062**
19	0.0132	0.0066	0.0025	0.0123	0.0039	0.0020	0.0160	0.0050	0.0035
	0.0183	**0.0120**	**0.0070**	**0.0150**	**0.0069**	**0.0043**	**0.0172**	**0.0067**	**0.0042**
20	0.0127	0.0074	0.0028	0.0115	0.0041	0.0023	0.0173	0.0052	0.0031
	0.0181	**0.0115**	**0.0071**	**0.0134**	**0.0055**	**0.0033**	**0.0209**	**0.0068**	**0.0042**
Outliers		11,20			13,14,15,16,17			14,15,16,18	
		17,19			**16,17,19**			**11,14,18,19,20**	

(*) Distribution shape-only indices, (**) Raw distribution indices

Table 9. The heterogeneity indices of LEDs at the current level of 210 mA.

LED-ID	T= +60 ℃			T= +70 ℃			T= +80 ℃		
	JSD	*WD*	MMD^2	*JSD*	*WD*	MMD^2	*JSD*	*WD*	MMD^2
Global index	0.0186(*)	0.0075	0.0050	0.0142	0.0041	0.0034	0.0260	0.0084	0.0069
	0.0146(**)	**0.0092**	**0.0043**	**0.0109**	**0.0037**	**0.0011**	**0.0164**	**0.0075**	**0.0024**
Local index									
21	0.0156	0.0065	0.0042	0.0205	0.0055	0.0080	0.0202	0.0072	0.0042
	0.0108	**0.0070**	**0.0041**	**0.0121**	**0.0039**	**0.0013**	**0.0157**	**0.0076**	**0.0023**
22	0.0132	0.0068	0.0029	0.0108	0.0031	0.0019	0.0204	0.0077	0.0047
	0.0115	**0.0076**	**0.0030**	**0.0093**	**0.0034**	**0.0011**	**0.0170**	**0.0080**	**0.0025**
23	0.0140	0.0058	0.0031	0.0101	0.0030	0.0019	0.0200	0.0062	0.0038
	0.0108	**0.0072**	**0.0021**	**0.0079**	**0.0032**	**0.0008**	**0.0153**	**0.0072**	**0.0029**
24	0.0195	0.0073	0.0054	0.0110	0.0032	0.0021	0.0226	0.0064	0.0045
	0.0136	**0.0093**	**0.0036**	**0.0089**	**0.0028**	**0.0006**	**0.0158**	**0.0063**	**0.0020**
25	0.0191	0.0075	0.0057	0.0166	0.0048	0.0054	0.0190	0.0063	0.0038
	0.0141	**0.0091**	**0.0049**	**0.0110**	**0.0033**	**0.0007**	**0.0135**	**0.0058**	**0.0016**
26	0.0243	0.0081	0.0070	0.0114	0.0035	0.0019	0.0247	0.0079	0.0067
	0.0162	**0.0085**	**0.0054**	**0.0102**	**0.0037**	**0.0011**	**0.0154**	**0.0065**	**0.0019**
27	0.0160	0.0063	0.0038	0.0125	0.0035	0.0023	0.0214	0.0070	0.0050
	0.0129	**0.0084**	**0.0042**	**0.0106**	**0.0035**	**0.0014**	**0.0156**	**0.0069**	**0.0028**
28	0.0174	0.0072	0.0057	0.0116	0.0035	0.0026	0.0294	0.0085	0.0096
	0.0118	**0.0076**	**0.0032**	**0.0090**	**0.0031**	**0.0008**	**0.0121**	**0.0059**	**0.0018**
29	0.0138	0.0060	0.0038	0.0122	0.0036	0.0029	0.0329	0.0097	0.0117
	0.0158	**0.0093**	**0.0046**	**0.0100**	**0.0035**	**0.0011**	**0.0128**	**0.0064**	**0.0019**
30	0.0141	0.0056	0.0032	0.0114	0.0033	0.0020	0.0232	0.0086	0.0078
	0.0141	**0.0084**	**0.0033**	**0.0094**	**0.0031**	**0.0008**	**0.0143**	**0.0072**	**0.0021**
Outliers		24,25,26,28			21,24,27,29			26,28,29,30	
		24,25,26,29,30			**21,26,27,29**			**21,22,23,27**	

(*) Distribution shape-only indices, (**) Raw distribution indices

These observations are consistent with the design of the SSADT, in which the initial stage is conducted at a lower temperature. Such a design does not compromise the assessment of degradation characteristics at higher temperatures, as the degradation process is cumulative and the physical mechanisms underlying voltage drift and material ageing are continuous across the stress range. Data collected at lower temperatures contribute to the estimation of early-stage degradation trends and help distinguish intrinsic material variability from stress-induced acceleration. Moreover, the stepwise design enables the separation of stress-dependent effects, allowing reliable evaluation of degradation dynamics and distributional parameters at each stress level, which is critical for modelling heterogeneity associated with both temperature and drive current. Table 6 also confirms that the estimated junction temperature differences closely align with the temperature steps applied in the tests, validating the experimental setup and supports the interpretation that observed heterogeneity in both initial voltage levels and degradation kinetics arises from intrinsic LED behaviour rather than from inconsistencies in applied stress.

4.2. Homogeneity hypothesis test

The results presented in Section 4.1 provide clear evidence that LED degradation heterogeneity is influenced by operating current and ambient temperature. Heterogeneity in the main degradation trends, reflected by differences in initial degradation levels and long-term degradation rates, is clearly evident from the explicit values reported in Table 3-5. Although the heterogeneity in the oscillatory components (IMFs) has been quantified descriptively in Table 6-8, a formal statistical assessment is required to determine whether the observed within-group variability is statistically significant.

For this analysis, the corresponding IMFs of LEDs were assumed to be independent and identically distributed samples. The null hypothesis was defined as H_0: "*The oscillatory components (IMFs) of LEDs within the same group are homogeneous,*" while the alternative hypothesis was H_1: "*The oscillatory components (IMFs) of LEDs within the same group are heterogeneous*." We employ IMF-based bootstrap procedure. The applied IMF-based bootstrap procedure offers several important advantages. First, it provides a quantitative, statistically rigorous evaluation of unit-to-unit variability,

preserving local degradation trends while enabling robust estimation of dispersion across LEDs. Second, it separates heterogeneity due to amplitude from differences in distribution shape or kinetics, allowing a nuanced understanding of degradation mechanisms under different operating conditions. Third, the bootstrap resampling approach is non-parametric and robust against small sample sizes or non-normal distributions, ensuring that the statistical conclusions are defensible. The testing procedure consisted of the following steps:

- Each IMF of each LED was divided into equal-sized blocks to preserve local degradation trends.
- Blocks of corresponding IMFs were pooled across LEDs within the same group.
- New IMFs for each LED were reconstructed by randomly selecting blocks from the pooled set.
- Test statistics were computed based on pairwise dispersion values derived from the reconstructed IMFs.
- P-values were estimated using bootstrap simulations with 2000 iterations.

Tables 10-12 summarise the results of the homogeneity tests for each LED group. The analysis indicates that all groups exhibit homogeneity in distribution shape across different temperature conditions, with no evidence to reject the null hypothesis. In contrast, statistically significant heterogeneity is predominantly associated with differences in the distribution mean. Specifically, LEDs operated at 210 mA show uniformity in mean, shape, and kinetics (Table 12), whereas LEDs at 525 mA exhibit mean-driven heterogeneity at +60 °C (Table 11), and LEDs at 1050 mA display heterogeneity in distribution mean at both +60 °C and +70 °C (Table 10). These insights ensure that degradation models reflect the intrinsic variability of the LED population rather than artefacts or measurement noise, enhancing both scientific rigor and practical relevance.

In summary, LEDs consistently exhibit heterogeneity in their degradation behaviour, reflected in differences in initial degradation values, and degradation rates across devices and operating conditions. In certain cases, the decomposition of the degradation signal further reveals non-homogeneous oscillatory components around the main degradation trend, indicating that variability is not limited to the long-term drift but also appears in the short-term micro-oscillations. These findings highlight that any degradation modelling framework must, at a minimum, account for heterogeneity in the degradation trend, rate, and initial state. In more complex scenarios, the modelling approach should also incorporate the heterogeneous oscillatory components around the trend to ensure an accurate and robust representation of the LED degradation process and lifetime prediction.

Table 10. Homogeneity hypothesis test results of LEDs at the current level 1050 mA.

Metrics	Value of test statistic	Critical value	Probability of test statistic	Null hypothesis test results
Raw distribution test				
T= +60 °C				
JSD	0.0137	0.0169	0.0005	Rejects
WD	0.0088	0.0127	0.0005	Rejects
MMD^2	0.0034	0.0056	0.0005	Rejects
T= +70 °C				
JSD	0.0121	0.0173	0.0005	Rejects
WD	0.0074	0.0110	0.0005	Rejects
MMD^2	0.0031	0.0051	0.0005	Rejects
T= +80 °C				
JSD	0.0165	0.0156	0.7496	Fails to reject
WD	0.0118	0.0132	0.0555	Fails to reject
MMD^2	0.0039	0.0042	0.0555	Fails to reject
Distribution shape-only test				
T= +60 °C				
JSD	0.0132	0.0139	0.2034	Fails to reject
WD	0.0088	0.0068	1.00	Fails to reject
MMD^2	0.0036	0.0024	1.00	Fails to reject
T= +70 °C				
JSD	0.0120	0.0175	0.0005	Rejects
WD	0.0073	0.0077	0.2689	Fails to reject
MMD^2	0.0041	0.0043	0.2539	Fails to reject
T= +80 °C				
JSD	0.0159	0.0141	0.9490	Fails to reject
WD	0.0118	0.0084	1.00	Fails to reject
MMD^2	0.0037	0.0027	1.00	Fails to reject

Table 11. Homogeneity hypothesis test results of LEDs at the current level 525 mA.

Metrics	Value of test statistic	Critical value	Probability of test statistic	Null hypothesis test results
Raw distribution test				
T= +60 °C				
JSD	0.0123	0.0178	0.0005	Rejects
WD	0.0083	0.0120	0.0005	Rejects
MMD^2	0.0045	0.0065	0.0005	Rejects
T= +70 °C				
JSD	0.0113	0.0143	0.0005	Rejects
WD	0.0059	0.0062	0.2459	Fails to reject
MMD^2	0.0033	0.0035	0.2546	Fails to reject
T= +80 °C				
JSD	0.0241	0.0202	0.9955	Fails to reject
WD	0.0107	0.0067	1,00	Fails to reject
MMD^2	0.0078	0.0042	1,00	Fails to reject
Distribution shape-only test				
T= +60 °C				
JSD	0.0119	0.0130	0.0555	Fails to reject
WD	0.0083	0.0072	0.9690	Fails to reject
MMD^2	0.0059	0.0050	0.9955	Fails to reject
T= +70 °C				
JSD	0.0111	0.0136	0.0005	Rejects
WD	0.0059	0.0044	0.9990	Fails to reject
MMD^2	0.0045	0.0034	1.00	Fails to reject
T= +80 °C				
JSD	0.0240	0.0209	0.9565	Fails to reject
WD	0.0109	0.0060	1.00	Fails to reject
MMD^2	0.0078	0.0069	1.00	Fails to reject

Table 12. Homogeneity hypothesis test results of LEDs at the current level 210 mA.

Metrics	Value of test statistic	Critical value	Probability of test statistic	Null hypothesis test results
Raw distribution test				
T= +60 °C				
JSD	0.0147	0.0147	0.4493	Fails to reject
WD	0.0080	0.0093	0.0255	Rejects
MMD^2	0.0040	0.0043	0.224	Fails to reject
T= +70 °C				
JSD	0.0114	0.0110	0.7216	Fails to reject
WD	0.0059	0.0037	1.00	Fails to reject
MMD^2	0.0013	0.0011	1.00	Fails to reject
T= +80 °C				
JSD	0.0237	0.0164	1.00	Fails to reject
WD	0.0130	0.0075	1.00	Fails to reject
MMD^2	0.0051	0.0024	1.00	Fails to reject
Distribution shape-only test				
T= +60 °C				
JSD	0.0135	0.0188	0.0005	Rejects
WD	0.0082	0.0075	0.8351	Fails to reject
MMD^2	0.0061	0.0056	0.8530	Fails to reject
T= +70 °C				
JSD	0.0113	0.0144	0.0005	Rejects
WD	0.0059	0.0041	1.00	Fails to reject
MMD^2	0.0060	0.0051	1.00	Fails to reject
T= +80 °C				
JSD	0.0234	0.0259	0.0880	Fails to reject
WD	0.0131	0.0084	1.00	Fails to reject
MMD^2	0.0049	0.0042	1.00	Fails to reject

5. Conclusions

In this article, we investigated the degradation heterogeneity of 10W LEDs using voltage data collected from optimized accelerated step-stress tests. The continuous measurements enabled the construction of large, high-resolution datasets suitable for statistical and reliability analyses.

A feature extraction approach combining Empirical Mode Decomposition, kernel density estimation, and divergence measures (JSD, WD, and MMD) was applied to evaluate degradation heterogeneity among LEDs under identical conditions. Rather than focusing on the root causes of heterogeneity or comparisons across different LED types, this study concentrated on quantifying heterogeneity within groups of LEDs operating under the same stress conditions. Two case studies were conducted to distinguish between heterogeneity in the main degradation trends, which reflects differences in initial degradation levels and long-term degradation rates; and heterogeneity in the oscillatory components (IMFs), which represent fluctuations around the trend and capture intrinsic variability within the degradation process. The results demonstrated that degradation heterogeneity is influenced by environmental factors and operating modes.

For future work, we plan to extend our experiments to different LED types and stress conditions to provide a more comprehensive characterization of degradation heterogeneity. Building on these insights, we aim to develop models that explicitly incorporate heterogeneity into LED degradation modelling and RUL prediction. Importantly, understanding and quantifying degradation heterogeneity can provide practical guidance for product design, reliability assessment, and predictive maintenance strategies in real-world LED applications.

Acknowledgment

This article has been prepared with support of the University of Defence, Brno, Czech Republic and in particular the "Partial development intention funding" VAROPS.

References

1. RIAC Automated Databook, Reliability Information Analysis Center. 2011 (https://www.quanterion.com/).
2. Liao G, Yin H, Chen M, Lin Z. Remaining useful life prediction for multi-phase deteriorating process based on Wiener process. Reliability Engineering & System Safety 2019; 207: 107361, https://doi.org/ 10.1016/j.ress.2020.107361.
3. You D, Liu S, Li F, Liu H, Zhang Y. Reliability Assessment Method Based on Small Sample Accelerated Life Test Data. Eksploatacja i Niezawodność – Maintenance and Reliability 2025; 27(1). https://doi.org/10.17531/ein/192170.
4. Nelson WB. Accelerated Testing: Statistical Models, Test Plans, and Data Analysis. New York: Wiley 2009.
5. International Electrotechnical Commission. IEC 62506:2023: Methods for product accelerated testing, 2nd ed. Geneva: IEC 2023.
6. Illuminating Engineering Society. IES LM-80: Measuring Lumen Maintenance of LED Light Sources. New York: Illuminating Engineering Society of North America 2014.
7. Zhang J, Yu X, Zhang H, Wang B, Wang J, Gu W, Zhang Y. Life prediction of LED lights by ADTs combined with luminance degradation and probability statistics. Journal of Luminescence 2025; 282: 121252, https://doi.org/10.1016/j.jlumin.2025.121252.
8. Herzog A, Hamon B, Myland P, Foerster P, Benkner S, Zandi B, Khanh TQ. Modeling Spectral LED Degradation Using an Unsupervised Machine Learning Approach. IEEE Access 2025; 13: 132440-132449, 2025, https://doi.org/10.1109/ACCESS.2025.3592806.
9. Alsharabi R, Almalki L, Abed F, Majid MA, Kittaneh OA. A Comparative Analysis of Statistical Modeling and Machine Learning Techniques for Predicting the Lifetime of Light Emitting Diodes From Accelerated Life Testing. IEEE Transactions on Electron Devices 2025; 72(4): 1864-1871, https://doi.org/10.1109/TED.2025.3535849.
10. Fan J, Jing Z, Cao Y, Ibrahim MS, Li M, Fan X, Zhang G. Prognostics of radiation power degradation lifetime for ultraviolet light-emitting diodes using stochastic data-driven models. Energy and AI 2021; 4: 100066, https://doi.org/10.1016/j.egyai.2021.100066.
11. Lokesh J, Kini SG, Padmasali AN. Color-Based Lifetime Estimation of LEDs Using Spectral Power Distribution Prediction Through Analytical and Machine Learning Models. IEEE Access 2024; 12: 87944-87953. https://doi.org/10.1109/ACCESS.2024.3418020.
12. Xia X, Stepanoff S, Haque A, Wolfe DE, Barke S, Wass PJ, Pearton SJ. ^{60}Co γ-irradiation of AlGaN UVC light-emitting diodes. Optical Materials 2023; 142: 114015, https://doi.org/10.1016/j.optmat.2023.114015.

13. Yan B, Teng T, Liu L, Wang G. Electrical stressing and self-heating effects on GaN-based LEDs' degradation under extremely low temperature. In 2018 19th International Conference on Electronic Packaging Technology, 2018; 168-175.
14. Hoang AD, Vintr Z, Vališ D, Mazurkiewicz D, An approach in determining the critical level of degradation based on results of accelerated test. Eksploatacja i Niezawodność – Maintenance and Reliability 2022; 24 (2): 330-337, https://doi.org/10.17531/ein.2022.2.14.
15. Padmasali AN, Lokesh J, Kini SG. Design of test method for analysis and estimation of LED luminaire lifetime performance under cycle based realistic operating conditions. IEEE Access 2024; 12: 87944-87953, https://doi.org/10.1109/ACCESS.2024.3418020.
16. Maarouf K, Roucoules C, Akrou KJ, Sao-Joao S, Klöcker H. Fatigue damage of automotive LEDs: Experimental approach and thermomechanical model. Microelectronics Reliability 2025; 171: 115799, https://doi.org/10.1016/j.microrel.2025.115799.
17. Lee YL, Lu MW. (2006). Damage-based models for step-stress accelerated life testing. Journal of Testing and Evaluation 2006; 34(6): 494-503, https://doi.org/10.1520/JTE100172.
18. Do GH, Lee SJ, Kim JS, Kim JY. Development of accelerated life testing apparatus for light-emitting diode therapy. IEEE Transactions on Device and Materials Reliability 2021; 21(4): 608-612, https://doi.org/10.1109/TDMR.2021.3121387.
19. Zhang JP, Liu C, Chen X, Cheng G L, Zhou AX (2014). Study on constant–step stress accelerated life tests in white organic light-emitting diodes. Luminescence 2014; 29(7): 933-937, https://doi.org/10.1002/bio.2644.
20. Jing Z, Ibrahim MS, Fan J, Fan X, Zhang G. Lifetime prediction of ultraviolet light-emitting diodes with accelerated Wiener degradation process. In 2019 20th International Conference on Thermal, Mechanical and Multi-Physics Simulation and Experiments in Microelectronics and Microsystems (EuroSimE), 2019; 1-8.
21. Cai M, Yang D, Mo Y, Huang J, Yin L, Yang L, Zhang G. Determining the thermal stress limit of LED lamps using highly accelerated decay testing. Applied Thermal Engineering 2016; 102: 1451-1461, http://doi.org/10.1016/j.applthermaleng.2016.04.012.
22. Wang XX, Jing L, Wang Y, Gao Q, Sun Q. The influence of junction temperature variation of LED on the lifetime estimation during accelerated aging test. IEEE Access 2018; 7: 4773-4781, http://doi.org/10.1109/ACCESS.2018.2885578.
23. Wang H, Zhao Y, Ma X. Mechanism equivalence in designing optimum step-stress accelerated degradation test plan under Wiener process. IEEE Access 2018; 6: 4440-4451, http://doi.org/10.1109/ACCESS.2018.2789518.
24. Sun Q, Huang G, Feng J, Pan Z (2012, June). Optimization of step stress accelerated degradation test plans based on MSE. In 2012 International Conference on Quality, Reliability, Risk, Maintenance, and Safety Engineering 2012; 962-965.
25. Liu G, Wang Z, Bao R, Mao Z, Ren K. Optimal design of step-stress accelerated degradation tests based on genetic algorithm and neural network. Quality Engineering 2024; 36(1): 66-79, https://doi.org/10.1080/08982112.2023.2225583.
26. Zhai Q, Li Y, Chen P. Modeling product degradation with heterogeneity: A general random-effects Wiener process approach. IISE Transactions 2024; 1-14, https://doi.org/10.1080/24725854.2024.2434125.
27. Zheng H, Yang J, Kang W, Zhao Y. Accelerated degradation data analysis based on inverse Gaussian process with unit heterogeneity. Applied Mathematical Modelling 2024; 126: 420-438, https://doi.org/10.1016/j.apm.2023.11.003.
28. Junxing L, Wang Z, Liu C, Qiu M. Accelerated degradation analysis based on a random-effect Wiener process with one-order autoregressive errors. Eksploatacja i Niezawodność – Maintenance and Reliability 2019; 21(2): 246-255. doi:10.17531/ein.2019.2.8.
29. Wen Y, Wu J, Yuan Y. Multiple-phase modeling of degradation signal for condition monitoring and remaining useful life prediction. IEEE Transactions on Reliability 2017; 66(3): 924-938, https://doi.org/10.1109/TR.2017.2710319.
30. Veloso GA, Loschi RH. Dynamic linear degradation model: Dealing with heterogeneity in degradation paths. Reliability Engineering & System Safety 2021; 210: 107446, https://doi.org/10.1016/j.ress.2021.107446.
31. Lokesh J, Kini SG, Padmasali AN, Mahesha MG. Reliability Estimation and Failure Analysis of LEDs with Various Currents and Correlated Color Temperatures for Identical Power Ratings: A Comparative Study. ACS omega 2025; 10(8): 8756-8766,

https://doi.org/10.1021/acsomega.5c00588.

32. Iero D, Merenda M, Carotenuto R, Pangallo G, Rao S, Brezeanu G, Corte F.G.D. A technique for improving the precision of the direct measurement of junction temperature in power light-emitting diodes. Sensors 2021; 21(9): 3113, https://doi.org/10.3390/s21093113.
33. Illuminating Engineering Society. IES TM-21-11: Projecting Long-Term Lumen Maintenance of LED Light Sources. New York: IESNA, 2011.
34. Vališ D, Forbelská M, Vintr Z, La QT, Kohl Z, Light emitting diode degradation and failure occurrence modelling based on accelerated life test. Engineering Failure. Analysis 2025; 169: 109200, https://doi.org/10.1016/j.engfailanal.2024.109200.
35. ShenZhen GeTian Optoelectronics Co. Specification for Approval: LED P10WW339910700 (ShenZhen GeTian Optoelectronics Co., 2013). Available from: https: //www.gme.cz, 2013.
36. Zhang Y, Meeker W. Bayesian methods for planning accelerated life tests. Technometrics 2006; 48(1):49-60, https://doi.org/10.1198/004017005000000373.
37. Lantieri P, Guérin F. Optimization of a Step-stress accelerated life test plan by genetic algorithm. Quality assurance 2009; 58.
38. EN 16798-1:2019: Energy Performance Building - Ventilation for Buildings - Part 1: Indoor Environmental Input Parameters for Design and Assessment of Energy Performance of Building Addressing Indoor Air Quality, Thermal Environment, Lighting, And Acoustics - Module M1-6. (CEN, 2019).
39. Chen YC. A tutorial on kernel density estimation and recent advances. Biostatistics & Epidemiology 2017; 1(1): 161-187, https://doi.org/10.48550/arXiv.1704.03924.
40. Silverman B.W. Density Estimation: for Statistics and Data Analysis, 1st ed. London: Chapman and Hall 1986.
41. Sheather SJ, Jones MC. A reliable data-based bandwidth selection method for kernel density estimation. Journal of the Royal Statistical Society: Series B (Methodological) 1991; 53(3): 683-690.
42. Huang NE, Shen Z, Long SR, Wu MC, Snin HH, Zheng Q, Yen NC, Tung CC, Liu HH. The empirical mode decomposition and the Hubert spectrum for nonlinear and non-stationary time series analysis. Proc R Soc A Math Phys Eng Sci 1998; 454(1971): 903–995. https://doi.org/10.1098/RSPA.1998.0193.
43. Zhou Y, Huang M. Lithium-ion batteries remaining useful life prediction based on a mixture of empirical mode decomposition and ARIMA model. Microelectronics Reliability 2016; 65: 265-273, https://doi.org/10.1016/j.microrel.2016.07.151.
44. Chen X, Liu Z. A long short-term memory neural network based Wiener process model for remaining useful life prediction. Reliability Engineering & System Safety 2022; 226: 108651, https://doi.org/10.1016/j.ress.2022.108651.
45. Zhang Y, Pan J, Li LK, Liu W, Chen Z, Liu X, Wang J (2023). On the properties of Kullback-Leibler divergence between multivariate Gaussian distributions. Advances in neural information processing systems 2023; 36: 58152-58165, https://doi.org/10.48550/arXiv.2102.05485.
46. Gurvich, V., & Naumova, M. (2025). Critical issues with the Pearson's chi-square test. Modern Mathematical Methods 2025; 3(2):101-109, https://doi.org/10.64700/mmm.75.
47. Mason DM, Schuenemeyer JH. A modified Kolmogorov-Smirnov test sensitive to tail alternatives. The annals of Statistics 1983; 933-946, https://doi.org/10.1214/aos/1176346259.
48. Menéndez ML, Pardo JA, Pardo L, Pardo MDC. The Jensen-Shannon divergence. Journal of the Franklin Institute 1997; 334(2): 307-318, https://doi.org/10.1016/S0016-0032(96)00063-4.
49. Villani C. Optimal transport: old and new. Berlin: springer, 2008.
50. Gretton A, Borgwardt KM, Rasch MJ, Schölkopf B, Smola A. A kernel two-sample test. The journal of machine learning research 2012; 13(1): 723-773.

51. Garreau D, Jitkrittum W, Kanagawa M. Large sample analysis of the median heuristic. 2017; https://doi.org/10.48550/arXiv.1707.07269.
52. Ljung GM, Box GE. On a measure of lack of fit in time series models. Biometrika 1978; 65(2): 297-303, https://doi.org/10.2307/2335207.
53. Wu Z, Huang NE. A study of the characteristics of white noise using the empirical mode decomposition method. Proceedings of the Royal Society of London, Series A: Mathematical, Physical and Engineering Sciences 2024; 460(2046): 1597-1611, https://doi.org/10.1098/rspa.2003.1221.
54. Klionskiy D, Kupriyanov M, Kaplun D. Signal denoising based on empirical mode decomposition. Journal of Vibroengineering 2017, 19(7): 5560-5570, https://doi.org/10.21595/jve.2017.19239.
55. Mann HB. Nonparametric tests against trend. Econometrica: Journal of the econometric society 1945; 194: 245-259, https://doi.org/10.2307/1907187.
56. Kendall MG. Rank correlation methods. Journal of the Institute of Actuaries. 1949; 75(1):140-141. https://doi.org/10.1017/S0020268100013019.
57. Montgomery DC, Peck EA, Vining GG. Introduction to linear regression analysis. New York: John Wiley & Sons, 2021.